# Ecosystem functioning is enveloped by hydrometeorological variability

Christoforos Pappas[1*], Miguel D. Mahecha[2,3], David C. Frank[4,5], Flurin Babst[4,6], and Demetris Koutsoyiannis[7]

[1] Département de géographie and Centre d'études nordiques, Université de Montréal, Montréal, QC, Canada

[2] Max Planck Institute for Biogeochemistry, 07745 Jena, Germany

[3] German Centre for Integrative Biodiversity Research (iDiv) Halle-Jena-Leipzig, Leipzig, Germany

[4] Swiss Federal Research Institute, WSL, Birmensdorf, Switzerland

[5] Laboratory of Tree-Ring Research, University of Arizona, AZ, USA

[6] W. Szafer Institute of Botany, Polish Academy of Sciences, Krakow, Poland

[7] Department of Water Resources and Environmental Engineering, School of Civil Engineering, National Technical University of Athens, Greece

[*] Corresponding author: Christoforos Pappas, Département de géographie, Université de Montréal, 520 ch. de la Côte Sainte-Catherine, Montréal, QC, H2V 2B8, CA (christoforos.pappas@umontreal.ca)

Terrestrial ecosystem processes, and the associated vegetation carbon dynamics, respond differently to hydrometeorological variability across time scales, and so does our scientific understanding of the underlying mechanisms. Long-term variability of the terrestrial carbon cycle is not yet well constrained and the resulting climate-biosphere feedbacks are highly uncertain. Here, we present a comprehensive overview of hydrometeorological and ecosystem variability from hourly to decadal time scales integrating multiple in-situ and remote-sensing datasets characterizing extra-tropical forest sites. We find that ecosystem variability at all sites is confined within a hydrometeorological envelope across sites and time scales. Furthermore, ecosystem variability demonstrates long-term persistence, highlighting ecological memory and slow ecosystem recovery rates after disturbances. However, simulation results with state-of-the-art process-based models do not reflect this long-term persistent behaviour in ecosystem functioning. Accordingly, we develop a cross-time-scale stochastic framework that captures hydrometeorological and ecosystem variability. Our analysis offers a perspective for terrestrial ecosystem modelling and paves the way for new model-data integration opportunities in Earth system sciences.

The atmosphere and biosphere are intrinsically coupled subsystems of the Earth[1]. Hydrometeorological conditions shape ecosystem processes, which, in turn, affect local, regional, and global climate (e.g., albedo feedbacks, modulations of land-atmosphere water and energy fluxes, seasonality in atmospheric $CO_2$). Hydrometeorological variability has been extensively studied[2] and short- and long-term variability of climate data have been widely assessed[3,4]. With some notable exceptions primarily focusing on shorter time scales and/or individual sites[5–9], much less work has undertaken to quantify the continuum of variability in ecosystem functioning across time scales. Key uncertainties remain in describing how variations in short-term physiological processes, such as photosynthesis[10], influence subsequent processes such as carbon allocation[11] and remobilization[12], and then, ultimately, inter-annual to long-term ecosystem variability.

Here, we present a comprehensive overview of the continuum of hydrometeorological and ecosystem variability, i.e., the variability of ecosystem process related to vegetation carbon dynamics, across sites and time scales. We analyse data from 23 extra-tropical forest sites covering different climatic zones and vegetation characteristics, and we examine time scales spanning five orders of temporal magnitude, from hourly to decadal variability (Figure 1).

“Variability” is intuitively quantified with the estimator of standard deviation ($\sigma$). The continuum of variability describes how $\sigma$ changes with averaging time scale ($k$), denoted as $\sigma^{(k)}$, and is illustrated in the double-logarithmic space log $k$ vs. log $\sigma^{(k)}$, a graph known as climacogram[13]. The advantages of this approach over other mathematically equivalent tools, such as power spectrum and variogram, are the very intuitive interpretation, the robust statistical estimation and the possibility to jointly analyse different datasets[14]. The continuum of variability represents the relative variability decay with time scale instead of using isolated values of individual variables or time scales. Thus, several cross-correlated datasets can be represented together, after applying appropriate linear transformations, to extend the continuum of variability to longer time scales. Moreover, we derive a mathematically tractable stochastic modelling framework that allows us to provide a quantitative interpretation and a parsimonious modelling of the observed cross-scale patterns of variability (see Methods).

Micrometeorological measurements of precipitation ($P$), air temperature ($T$), shortwave radiation ($R$), and vapour pressure deficit ($D$) are used to describe hydrometeorological variability at the analysed forest sites from hourly to annual time scales. The continuum of hydrometeorological variability is extended to the decadal time scale using reanalysis data for *P*, *T*, *R*, and *D,* extracted from the examined locations (see Methods). Ecosystem variability is quantified using essential ecosystem variables, namely, long-term (≥10 yr) eddy covariance flux data of hourly net ecosystem exchange of $CO_2$ between land surface and atmosphere (NEE), monthly remote sensing measurements of leaf area index (LAI) and fraction of absorbed photosynthetically active radiation (FPAR), and annual tree ring widths (TRW) and site-level above ground biomass increment estimates (AGB), available at five of the analysed forests (Figure 1b; see Methods).

We construct the relative ecosystem variability continuum by concatenating the time scales of NEE variability with those of LAI, FPAR, TRW, and AGB data. We scrutinize their common relative variability decay patterns, even if the variables themselves reflect different aspects of ecosystem processes and dynamics. NEE data capture high frequency variations of ecosystem carbon fluxes exchanged between atmosphere and the biosphere[15] and describe ecosystem variability from hourly to inter-annual time scales[5–8]. Today, the longest analysed NEE time series is approx. 20 years (Figure 1c), allowing characterization of the ecosystem variability continuum from hourly up to biennial time scales (see Methods). Remote sensing data of vegetation indices, such as LAI and FPAR, are tightly related to vegetation carbon dynamics (e.g., light use efficiency models use FPAR to derive vegetation carbon fluxes[16] and stocks[17]). Thus, these vegetation indices can be used as proxies of ecosystem functioning extending the ecosystem variability continuum from intra-annual to triennial time scales with 30-year-long LAI and FPAR time series[18]. At these time scales, carbon fluxes and remote sensing vegetation indices should be tightly interconnected and can therefore be expected to show similar patterns of variability. At longer time scales, TRW and AGB data reveal annual tree growth and biomass dynamics and provide estimates of forest carbon dynamics that converge to observed NEE across several forests worldwide[19–22]. Time series length of TRW and AGB at the five analysed forest sites ranges from 41 to 111 years[20] (Figure 1b), thus the annual to decadal ecosystem variability at these sites can be sufficiently captured (see Methods).

## RESULTS

We find that most hydrometeorological drivers display similar pattern of variability from hourly to inter-annual time scales across all sites, except for $P$ which is also well-known for its high spatial variability[3,4] (Figure 2b-e). However, such convergence across sites is not reflected in the ecosystem variability (i.e., NEE, Figure 2a, as well as individual NEE components, Figure S3). Although the continuum of ecosystem variability follows a similar pattern across all the analysed sites (i.e., consistent drops in standard deviation at specific time scales), site-specific vegetation phenology dictates the magnitude of standard deviation at intra-annual time scales. Seasonal ecosystem variability at deciduous forest sites is thus larger compared to evergreen forest sites. This is a result of the pronounced phenological cycles of the former, whereas at forest sites with mixed vegetation phenology, seasonal ecosystem variability falls between the variability of evergreen and deciduous forest sites (Figure 2a). Furthermore, NEE, $R$, $T$, and $D$ with pronounced periodical cycles at diurnal or annual scales show characteristic drops in their standard deviation at these very time scales, together with discontinuities (spikes) at half the period of the harmonic cycle ($\tau/2$), as well as at time scales $k$ equal to $m\tau/2$, $m \in \mathbf{N}$. This pattern is caused by the interplay of daily and annual harmonic cycles and can be described analytically (see Methods).

By superimposing the continuum of variability of the analysed ecosystem variables, namely NEE, LAI, FPAR, TRW, and AGB, we obtain a composite cross-scale ecosystem variability continuum from one hour to one decade (Figure 3a). The composed variability continuum is consistent as confirmed by the close match of the variability of individual ecosystem variables at the overlapping time scales (Figure 3a; see Figure S10 for a quantitative assessment). More specifically, as illustrated in Figure 3a for an exemplary forest site, the standard deviation of NEE, as well as that of LAI and FPAR from two independent remote sensing products, overlap at monthly to inter-annual time scales. Similarly, the standard deviation of TRW and AGB matches closely the standard deviation of NEE at the annual to biennial time scales and the standard deviation of LAI, FPAR at annual to triennial time scales (Figure 3a). Therefore, despite the fact that different variables represent specific, yet tightly interwoven aspects of ecosystem functioning, the overall ecosystem variability across time scales may now be approximated by the variability of NEE, LAI, and TRW data for hourly-to-monthly, monthly-to-annual, and annual-to-decadal time scales, respectively (Figure 3a). Micrometeorological measurements, compiled together with reanalysis climate data, describe the continuum of variability of $P$, $T$, $R$, and $D$ from one hour to one decade (Figure 3b). The use of several reanalysis datasets allows us to provide a better description of the hydrometeorological variability, accounting for uncertainties due to different products and gridding algorithms[23] (see Methods).

Overall, we find that ecosystem variability is confined within a hydrometeorological envelope that describes the range of variability of the available resources, i.e., water and energy (Figure 4). The hydrometeorological envelope emerges from the continua of variability of individual hydrometeorological variables (e.g., Figure 3b). For an exemplary site, a one-order-of-magnitude increase of the time scale (e.g., from one day to one month; x-axes Figure 3) leads to a fivefold decrease in the standard deviation of precipitation (lower bound of the envelope) and to a mild decrease in the standard deviation of temperature by approx. 10 % (upper bound of the envelope; y-axis Figure 3b), while the standard deviation of ecosystem functioning exhibits a gentle decrease by approx. 15 % (y-axis Figure 3a). Figure 4 illustrates the hydrometeorological envelope of ecosystem variability continua at five European forest sites where TRW and AGB data are available (Figure 1b). The slopes of the entire continuum of *P*, *T*, *R*, and *D* variability, when compared to those of the ecosystem variability continua at the 23 analysed forest sites, provide a quantitative description of the hydrometeorological envelope in which ecosystem variability is confined (Figure S15). Steep slopes of *P* variability describe the lower limit of the hydrometeorological envelope and gentle slopes of *R* and *T* variability the upper limit, while the slopes of ecosystem variability continua fall within the range of slopes of the hydrometeorological variables (Figure S15).

Furthermore, ecosystem variability demonstrates long-term persistence. Although absolute values of ecosystem variability differ across sites as a result of different climate, vegetation composition, and stand characteristics, the temporal dependences exhibit the same behaviour across the entire range of analysed time scales (Figure 4). The lower end of the continuum of ecosystem variability shows gentle slopes, indicating long-term persistence in ecosystem functioning (Figure 5a). Yet, simulation results with state-of-the-art Dynamic Global Vegetation Models (DGVMs; TRENDY multi-model ensemble[24]; see Methods) do not reflect this pattern (Figure 5b and Figure S12, as well as Figure S13d for TRENDY-simulated net primary productivity, NPP). TRENDY-derived ecosystem variability continuum is consistent with the composite of observations at intra-annual time scales, yet diverges significantly at inter-annual or longer time scales. At these scales, ecosystem variability simulated with the TRENDY multi-model ensemble presents a much steeper decrease than what observations indicate (Figure 5, Figure S13). Thus, the simulated continua of both NEE (Figure 5b) and NPP (Figure S13d) variability approach the lower limit of the hydrometeorological envelope (i.e., $P$ variability), with the former exhibiting steeper variability decay than the latter, and contradict observational evidence of long-term persistence in ecosystem functioning (i.e., upper limit of the envelope, close to $R$ and $T$ variability).

To further investigate the properties and controls on the ecosystem and hydrometeorological variability, we develop a stochastic modelling framework to simulate the observed patterns of variability across time scales. A combination of deterministic harmonics and stochastic processes (Figure 6; see Methods) allows us to analytically describe the observed patterns (e.g., the imprint of harmonic cycles on ecosystem variability across time scales or the magnitude of its low frequency variability), and to further investigate the properties and controls on ecosystem and hydrometeorological variability. Diurnal and seasonal cycles correspond to variability continua of harmonic functions with periods $T_1$=24 h ($\sigma_{T_1}^{(k)}$) and $T_2$=1 yr ($\sigma_{T_2}^{(k)}$), respectively (Figure 6a). The deterministic harmonics are then combined with three structurally different stochastic processes, namely, a purely random process (white noise; abrupt drop in standard deviation as time scale increases, i.e., corresponding to processes with no memory), a Markovian process (autoregressive model of order one, AR(1), i.e., reflecting processes with short-term persistence), and a Hurst-Kolmogorov (HK) process with long-term persistence (Figure 6b). The continuum of variability of the latter ($\sigma_{\mathrm{HK}}^{(k)}$) combined with that of the two harmonic functions, $\sigma_{T_1}^{(k)}$ and $\sigma_{T_2}^{(k)}$ (i.e., $a\sigma_{T_1}^{(k)} + b\sigma_{T_2}^{(k)} + c\sigma_{\mathrm{HK}}^{(k)}$, where $a$, $b$, and $c$ are weighting factors) are fully sufficient to describe the observed ecosystem and hydrometeorological variability from hourly to decadal time scales (Figure 6c,d; see Methods). The close agreement between simulated and observed patterns of ecosystem variability brings quantitative evidence on the magnitude of long-term persistence in ecosystem functioning (Figure S15).

## DISCUSSION

As time scale increases, hydrometeorological and ecosystem variability decreases. However, hydrometeorological conditions frame an envelope constraining the continuum of ecosystem variability within its boundaries. We find that ecosystem variability exhibits a gentle decrease as time scale increases, highlighting the impact of low frequency variability in ecosystem functioning. Precipitation defines the lower limit and energy (i.e., temperature and radiation) the upper limit of plausible variability regimes, with the resulting ecosystem variability being confined within these boundaries across sites and time scales. Low frequency ecosystem variability has pronounced implications for our understanding of ecosystem stability and resilience[25], because it denotes ecological memory[26,27] and slow ecosystem recovery rates after disturbances[25,28]. For instance, a steep decay of ecosystem variability with time scale (i.e., processes with no- or short-memory) would indicate fast ecosystem recovery rates after disturbances (i.e., enhanced resilience), but both theoretical[26] and observational evidence reported in the ecological literature rather suggest substantial memory effects in ecosystem functioning (e.g. after drought stress[27]). This pattern epitomizes the slow recovery rates of forest ecosystems and their susceptibility to tipping points[25]. It is also expected that changes in the hydrometeorological drivers, for example in the frequency and severity of climate extremes[1], could alter the hydrometeorological envelope and affect the cross-scale continuum of ecosystem variability[29,30].

DGVMs offer a process-based representation of terrestrial ecosystem dynamics, integrating our current ecophysiological understanding. However, a bottom-up modelling of terrestrial ecosystem functioning is challenging, particularly when long-term predictions are envisioned[31]. While DGVMs capture intra-annual ecosystem variability adequately, ecosystem variability simulated with the TRENDY multi-model ensemble[24] does not reflect the pattern derived from the composed observational data at inter-annual to decadal time scales. We acknowledge that the composite of cross-scale ecosystem variability is approximated using various datasets of vegetation carbon dynamics while it ideally should be based on multi-decadal NEE measurements which are, however, not available today. Yet, at long time-scales net exchange rates of ecosystems are expected to have a similarly persistent behaviour compared to the tree ring width variations. Hence, the observed discrepancy leads us to the hypothesis that processes influencing low frequency variability in ecosystem functioning are either insufficiently constrained or not included in current DGVMs. For example, stand demographic processes and the resulting age-related variability in tree growth are rarely simulated in many DGVMs[32], with some notable exceptions[33,34]. However, apart from the five analysed forest sites where tree ring data are available, low frequency variability is also revealed with remote sensing data from the remaining 18 sites (Figure S15). This underlines that, apart from stand demography, other factors will contribute to persistence in ecosystem functioning. In particular, the interplay of plant ecophysiological processes relating carbon supply (i.e., photosynthesis; source activity) to carbon demand (i.e., tissue expansion; sink activity) is yet to be realistically described in DGVMs[35–37] and is known to significantly affect the low frequency variability in the terrestrial carbon cycle. A mechanistic understanding of the interplay between environmental drivers (e.g., water[38], $CO_2$[39], nutrients[40]) and ecophysiological response (resource allocation and remobilization[11,12], plant acclimation and plasticity[41,42]) is still to be consolidated, leading to well-documented structural and parameterizations issues in DGVMs[37,43] that could eventually explain the steep decay in the TRENDY-simulated ecosystem variability continuum. Moreover, the mismatch between the spatial scale of DGVMs input (e.g., climate forcing, initial conditions) and the resolution of the DGVMs simulation grid hampers the parameterization of fine-scale processes and results in aggregation biases in the simulated terrestrial carbon dynamics[44,45]. Finally, several processes with well-documented impact on terrestrial carbon fluxes and stocks are also not yet adequately represented in state-of-the-art DGVMs (e.g., leaf mesophyll conductance[46], carbon turnover rates[47], soil microbial activity[48]), and may affect cross-scale ecosystem variability.

We derive an analytical model, combining deterministic harmonics and stochastic processes, that represents major mechanisms and uncertainties and mimics the observed pattern of hydrometeorological and ecosystem variability. Additional natural (e.g., wildfires, insect outbreaks) or anthropogenic (e.g., forest management) mechanisms, that may affect the variability of certain ecosystems, can be also incorporated in the aforementioned framework by including theoretical representations of their cross-scale variability according to the observed patterns. This stochastic modelling framework offers a parsimonious and mathematically tractable approach for understanding and modelling ecosystem variability across sites and time scales, overcoming the aforementioned limitations of DGVMs. Furthermore, this framework well-reflects the observed ecological memory, an inherent property of ecosystem functioning, enhancing therefore the ecological realism in numerical simulations.

The presented analysis offers a perspective for understanding and modelling the variability of the terrestrial carbon cycle and paves the way for new model-data integration opportunities in Earth system sciences. DGVMs are incorporated in Earth System Models (ESMs) to simulate the terrestrial ecosystem dynamics and climate-biosphere feedbacks[49]. Thus, poorer fidelity of low frequency variability in the former will be propagated to simulation results with the latter, leading to potential biases in the resulting climate projections[50]. While model-data comparisons in terms of relative, rather than absolute, variability are widespread, so far the focus has been on individual time scales (e.g., monthly or annual anomalies of observed vs. simulated variables). However, analysing and modelling the interplay between hydrometeorological drivers and ecosystem response requires developing a joint framework across multiple sites and time scales. Hence, we advocate to formalize and implement a cross-scale model-data integration approach. The presented continuum of ecosystem variability offers an independent emerging observational constraint for ESMs[49] and the projected terrestrial carbon source-sink dynamics[24]. Moreover, the derived hydrometeorological envelope defines the boundaries of plausible climate-carbon cycle sensitivities allowing for a predictive understanding of long-term terrestrial ecosystem response and climate-biosphere feedbacks[1,31].

## METHODS

### Datasets

*Hydrometeorological drivers.* Time series of *P*, *T*, *R*, and *D* are used to quantify hydrometeorological variability (Table S2). Micrometeorological data, obtained from FLUXNET2015 (December 2015 release; http://fluxnet.fluxdata.org/data/fluxnet2015-dataset/fullset-data-product/), are compiled together with time series of the following reanalysis gridded products: ERA Interim[51], NCEP I[52] and II[53], 20th century reanalysis version v2c[54–56], CRU TS 1.2[57], CRU TS 3.23[58], and CRU-NCEPv4. The latter is a combination of CRU TS 3.21 and NCEP I, and is used for climate forcing of TRENDY simulations[24]. Grid cells that correspond to the locations of the eddy covariance forest sites are selected (supporting information S1.1 and S1.2).

*Ecosystem response*. Ecosystem variability is quantified based on multivariate proxies of ecosystem functioning (Table S1), consisting of: (i) hourly NEE data (Table S3); (ii) monthly LAI and FPAR time series from grid cells corresponding to the location of the eddy covariance forest sites, provided by the Moderate Resolution Imaging Spectroradiometer Two-stream Inversion Package[59] (MODIS TIP; time period: 2001-2014, Figure S5) and the third generation of Global Inventory Modelling and Mapping Studies[18] (GIMMS 3g; time period: 1981-2011, Figure S6); and (iii) TRW (Figure S7) and AGB[20] (Figure S8) available at five European sites (Figure 1b). The pattern of variability of the partitioned hourly NEE data to gross primary productivity and ecosystem respiration is also examined (supporting information S1.1.3). Moreover, the observed pattern of ecosystem variability is compared with simulated monthly

NEE from TRENDY v1 multi-model ensemble[24] (Figure 5) as well as additional simulated variables (supporting information and S1.6).

**Statistical analysis**

*Empirical climacograms.* The continuum of hydrometeorological and ecosystem variability is quantified by examining how the (sample) standard deviation ($\sigma^{(k)}$) of various hydrometeorological and ecosystem variables changes across averaging time scales ($k$). The values of $k$ range from the original temporal resolution of each dataset ($\Delta$) to $L/10$ where $L$ is the total length of the time series[13], allowing therefore for at least 10 values for the estimation of $\sigma^{(k)}$ at $k=L/10$. In order to compare hydrometeorological and ecosystem variability across sites and variables, data are standardized, i.e., zero mean and unit variance at the original time scale (e.g., $\Delta$ = 1 h for micrometeorological and NEE measurements, Figure 2a; $\Delta$ = 1 mon for LAI and FPAR, Figure S5, S6; and $\Delta$ = 1 yr for TRW and AGB, Figure S9).

*Composite climacograms*. Linear transformations are applied to construct the combined continuum of ecosystem and hydrometeorological variability. Cross-correlated variables that reflect ecosystem functioning at different time scales can be combined in a single climacogram after applying appropriate linear transformations. This allows us to compare how the standard deviation of different processes varies and co-varies across ecosystems and time scales. For example, if the process of interest is ecosystem functioning ($y(t)$; where $t$ denotes time) then NEE, LAI, FPAR, TRW, AGB can be seen as proxies of $y(t)$. These proxies are intrinsically related, and, as an approximation, we can assume that they are linearly connected. In other words, $y(t) = ax(t) + b$, where $x(t)$ can be any of the proxy variables NEE, LAI, FPAR, TRW, AGB. Thus, it follows that $\sigma_y^{(k)} = a\sigma_x^{(k)}$. The close match of the variability of individual ecosystem variables at the overlapping time scales supports this approximation (Figure 3a and Figure S10). Moreover, theoretical and observational evidence demonstrate the applicability of light use efficiency models to linearly relate LAI and FPAR with carbon uptake, thus capturing the variability of vegetation carbon fluxes[16] and stocks[17].

More specifically, LAI and FPAR data are transformed so that $\sigma_{\mathrm{LAI,FPAR}}^{(k=1\ \mathrm{mon})} = \sigma_{\mathrm{NEE}}^{(k=1\ \mathrm{mon})}$ and TRW and AGB data are transformed so that $\sigma_{\mathrm{TRW,AGB}}^{(k=1\ \mathrm{yr})} = \sigma_{\mathrm{LAI}}^{(k=1\ \mathrm{yr})}$. Reanalysis hydrometeorological data are transformed so that the standard deviation of each hydrometeorological variable at the original time scale ($\Delta_i$) matches the standard deviation of the same variable from the micrometeorological measurements at this time scale, e.g., for the case of precipitation $\sigma_{\mathrm{reanalysis},P}^{(k=\Delta_i)} = \sigma_{\mathrm{micromet},P}^{(k=\Delta_i)}$ (Figure 3b). The increments in the x-axis of the hydrometeorological envelope depicted in Figure 4 are coarser than Figure 3b for the sake of figure's clarity, thus the drops in standard deviation due to the diurnal and seasonal harmonic cycles are not visible (cf. Figure 3b).

*Theoretical climacograms.* Once the underlying process is known, its continuum of variability can be derived analytically[13]. Figure 6a depicts the theoretical variability across time scales for deterministic harmonic processes with different periods, $\tau$, while Figure 6b illustrates the variability across time scales for three structurally different stochastic process. The standard deviation as a function of $k$ of a single harmonic process is given by:

$$\sigma_{\tau}^{(k)} = \frac{\tau}{\pi k}\left|sin\frac{\pi k}{\tau}\right|, \qquad \text{for } k \neq \left(m+\frac{1}{2}\right)\tau, \text{where } m \in \mathbf{N}^0 \tag{1}$$

For $k = \left(m+\frac{1}{2}\right)\tau$ there is a discontinuity in the continuum of variability (e.g., spikes for $k$=12 h for the case of diurnal cycle, or $k$=6 mon for the seasonal cycle in Figure 3; supporting information S4). A purely random process (white noise; WN) and two widely used stochastic processes in geophysics, namely, (i) a Markovian process characterized by short-term persistence and (ii) a Hurst-Kolmogorov (HK) process with long-term persistence, are also examined. The standard deviation of WN decays with *k* as follows:

$$\sigma_{\mathrm{WN}}^{(k)} = \frac{\sigma}{\sqrt{k}} \tag{2}$$

where $\sigma$ denotes the standard deviation at the original time scale. For Markovian process, described by an autoregressive model of order one, AR(1) with lag-1 autocorrelation ($\rho$), $\sigma^{(k)}$ is given by:

$$\sigma_{\mathrm{AR(1)}}^{(k)} = \frac{\sigma}{\sqrt{k}} \sqrt{\frac{(1-\rho^2) - 2\rho(1-\rho^k)/k}{(1-\rho)^2}} \tag{3}$$

while for HK process $\sigma^{(k)}$ is equal to:

$$\sigma_{\mathrm{HK}}^{(k)} = k^{H-1}\sigma \tag{4}$$

where $H$ is the Hurst coefficient ($H = 0.5[\log_2(\rho+1)+1]$). The continuum of variability of AR(1) and HK process present distinct patterns. The former is characterized by a fast decay that is equal to WN for large time scales, while the latter shows gentle slopes as a result of long-term persistence (Figure 5b).

*Model fitting.* Theoretical climacograms are fitted to empirical estimates of standard deviation ($\sigma^{(k)}$) accounting for biases in $\sigma^{(k)}$ due to sample size ($L$). Bias in $\sigma^{(k)}$ can be estimated *a priori* analytically[13] and is equal to:

$$\mathrm{E}\left[\sigma^{(k)}\right] = \frac{\sigma_y^{(k)} - \sigma_y^{(L)}}{1 - k/L}$$

A model, $\sigma_y^{(k)}$, is assumed based on a linear combination of $\sigma_{T_1}^{(k)}$, $\sigma_{T_2}^{(k)}$, $\sigma_{\mathrm{WN}}^{(k)}$, $\sigma_{\mathrm{AR(1)}}^{(k)}$, $\sigma_{\mathrm{HK}}^{(k)}$, i.e.,

$$\sigma_y^{(k)} = \begin{cases} a\sigma_{T_1}^{(k)} + b\sigma_{T_2}^{(k)} + c\sigma_{\mathrm{WN}}^{(k)} \\ a\sigma_{T_1}^{(k)} + b\sigma_{T_2}^{(k)} + c\sigma_{\mathrm{AR(1)}}^{(k)} \\ a\sigma_{T_1}^{(k)} + b\sigma_{T_2}^{(k)} + c\sigma_{\mathrm{HK}}^{(k)} \end{cases}$$

Weighting factors $a$, $b$, $c$, as well as lag-1 autocorrelation ($\rho$), for the case of AR(1), or Hurst coefficient ($H$), for the case of the HK process, are fitting parameters adjusted so that the sum of squared errors is minimized numerically (supporting information S3). For the model fitting of ecosystem variability continuum (Figure 6c), theoretical models are fitted to the composite empirical ecosystem continuum as described by NEE (1 h – 1 mon), LAI 3g (1 mon – 1 yr), and TRW (1 yr – 10 yr) where available. Model fitting for each hydrometeorological variable (Figure 6d) is conducted by fitting theoretical models to the mean empirical continuum of variability estimated as the mean of the micrometeorological, CRU-NCEPv4, and 20th century reanalysis version v2c datasets (supporting information S2). These three datasets are selected due the large overlap in the analysed time scales (Figure 3b).

**Data availability**

The micrometeorological, eddy covariance and remote sensing data that support the findings of this study are available from public repositories (see supporting information S1). Tree-ring widths and site-level above ground biomass increment estimates used in this study are available upon reasonable request to D.C.F. and F.B., respectively.

**Code availability**

The analysis was conducted in R version 3.3.2 and the scripts of the analysis are available from the corresponding author upon reasonable request.

**ACKNOWLEDGEMENTS.** This work used eddy covariance data acquired and shared by the FLUXNET community, including these networks: AmeriFlux, AfriFlux, AsiaFlux, CarboAfrica, CarboEuropeIP, CarboItaly, CarboMont, ChinaFlux, Fluxnet-Canada, GreenGrass, ICOS, KoFlux, LBA, NECC, OzFlux-TERN, TCOS-Siberia, and USCCC. The FLUXNET eddy covariance data processing and harmonization was carried out by the ICOS Ecosystem Thematic Center, AmeriFlux Management Project and Fluxdata project of FLUXNET, with the support of CDIAC, and the OzFlux, ChinaFlux and AsiaFlux offices. We thank the participants of the TRENDY project, namely, Peter Levy (Hyland), Stephen Sitch and Chris Huntingford (JULES /TRIFFID), Benjamin Poulter (LPJ), Anders Ahlström (LPJ-GUESS), Sam Levis (NCAR-CLM4), Nicolas Viovy, Sönke Zaehle (OCN), Mark Lomas (SDGVM) and Ning Zeng (VEGAS), who made their simulations results (TRENDY v1, experiment S2), freely available. C.P. acknowledges the support of the Stavros Niarchos Foundation and the ETH Zurich Foundation (grant P2EZP2_162293) through a Swiss National Science Foundation (SNSF) Early Postdoc.Mobility fellowship. M.D.M., F.B. and D.C.F. acknowledge funding from the European Union via the Horizon 2020 project “BACI” (grant 640176). F.B. acknowledges funding from the Swiss National Science Foundation (grant P300P2_154543).

**AUTHOR CONTRIBUTIONS.** C.P. designed the study, conducted the analysis, and wrote the manuscript with input from M.D.M. and D.K. D.C.F. provided the tree ring width data and F.B. the above ground biomass increment data. All authors contributed to editing the manuscript.

**COMPETING INTERESTS.** The authors declare no competing financial interests.

## References


1. IPCC. *Climate Change 2013: The Physical Science Basis. Contribution of Working Group I to the Fifth Assessment Report of the Intergovernmental Panel on Climate Change*. (Cambridge University Press, 2013).

2. Mitchell, J. M. An Overview Of Climate Variability And Its Causal Mechanisms. *Quat. Int.* **6,** 481–493 (1976).

3. Franke, J., Frank, D., Raible, C. C., Esper, J. & Brönnimann, S. Spectral biases in tree-ring climate proxies. *Nat. Clim. Chang.* **3,** 360–364 (2013).

4. Markonis, Y. & Koutsoyiannis, D. Scale-dependence of persistence in precipitation records. *Nat. Clim. Chang.* **6,** 1–3 (2016).

5. Baldocchi, D., Falge, E. & Wilson, K. A spectral analysis of biosphere-atmosphere trace gas flux and meteorologiacal variables across hour to multi-year time scales. *Agric. For. Meteorol.* **2915,** 1–27 (2000).

6. Katul, G. *et al.* Multiscale analysis of vegetation surface fluxes: from seconds to years. *Adv. Water Resour.* **24,** 1119–1132 (2001).

7. Mahecha, M. D. *et al.* Characterizing ecosystem-atmosphere interactions from short to interannual time scales. *Biogeosciences* **4,** 743–758 (2007).

8. Stoy, P. C. *et al.* Biosphere-atmosphere exchange of $CO_2$ in relation to climate: a cross-biome analysis across multiple time scales. *Biogeosciences* **6,** 2297–2312 (2009).

9. Mueller, K. L., Yadav, V., Curtis, P. S., Vogel, C. & Michalak, A. M. Attributing the

variability of eddy-covariance $CO_2$ flux measurements across temporal scales using geostatistical regression for a mixed northern hardwood forest. *Global Biogeochem. Cycles* **24,** (2010).

10. Farquhar, G. D., von Caemmerer, S. & Berry, J. A. A biochemical model of photosynthetic $CO_2$ assimilation in leaves of C3 species. *Planta* **149,** 78–90 (1980).

11. Franklin, O. *et al.* Modeling carbon allocation in trees: a search for principles. *Tree Physiol.* **32,** 648–66 (2012).

12. Hartmann, H. & Trumbore, S. Understanding the roles of nonstructural carbohydrates in forest trees - from what we can measure to what we want to know. *New Phytol.* (2016). doi:10.1111/nph.13955

13. Koutsoyiannis, D. Generic and parsimonious stochastic modelling for hydrology and beyond. *Hydrol. Sci. J.* **6667,** 1–6 (2015).

14. Dimitriadis, P. & Koutsoyiannis, D. Climacogram versus autocovariance and power spectrum in stochastic modelling for Markovian and Hurst–Kolmogorov processes. *Stoch. Environ. Res. Risk Assess.* (2015). doi:10.1007/s00477-015-1023-7

15. Baldocchi, D. *et al.* FLUXNET: A New Tool to Study the Temporal and Spatial Variability of Ecosystem-Scale Carbon Dioxide, Water Vapor, and Energy Flux Densities. *Bull. Am. Meteorol. Soc.* **82,** 2415–2434 (2001).

16. Hilker, T., Coops, N. C., Wulder, M. A., Black, T. A. & Guy, R. D. The use of remote sensing in light use efficiency based models of gross primary production: A review of current status and future requirements. *Sci. Total Environ.* **404,** 411–423 (2008).

17. Myneni, R. B. *et al.* A large carbon sink in the woody biomass of Northern forests. *Proc. Natl. Acad. Sci. U. S. A.* **98,** 14784–9 (2001).

18. Zhu, Z. *et al.* Global Data Sets of Vegetation Leaf Area Index (LAI)3g and Fraction of Photosynthetically Active Radiation (FPAR)3g Derived from Global Inventory Modeling and Mapping Studies (GIMMS) Normalized Difference Vegetation Index (NDVI3g) for the Period 1981 to 2. *Remote Sens.* **5,** 927–948 (2013).

19. Rocha, A., Goulden, M., Dunn, A. & Wofsy, S. On linking interannual tree ring variability with observations of whole-forest $CO_2$ flux. *Glob. Chang. Biol.* **12,** (2006).

20. Babst, F. *et al.* Above-ground woody carbon sequestration measured from tree rings is coherent with net ecosystem productivity at five eddy-covariance sites. *New Phytol.* **201,** 1289–1303 (2014).

21. Campioli, M. *et al.* Evaluating the convergence between eddy-covariance and biometric methods for assessing carbon budgets of forests. *Nat. Commun.* **7,** 13717 (2016).

22. Delpierre, N., Berveiller, D., Granda, E. & Dufrene, E. Wood phenology, not carbon input, controls the interannual variability of wood growth in a temperate oak forest. *New Phytol.* **210,** 459–470 (2016).

23. Cavanaugh, N. R. & Shen, S. S. P. The effects of gridding algorithms on the statistical moments and their trends of daily surface air temperature. *J. Clim.* **28,** 9188–9205 (2015).

24. Sitch, S. *et al.* Recent trends and drivers of regional sources and sinks of carbon dioxide. *Biogeosciences* **12,** 653–679 (2015).

25. Scheffer, M., Carpenter, S. R., Dakos, V. & Nes, E. H. van. Generic Indicators of

Ecological Resilience: Inferring the Chance of a Critical Transition. *Annu. Rev. Ecol. Evol. Syst.* **46,** 145–167 (2015).

26. Ogle, K. *et al.* Quantifying ecological memory in plant and ecosystem processes. *Ecol. Lett.* **18,** 221–235 (2015).

27. Anderegg, W. R. L. *et al.* Pervasive drought legacies in forest ecosystems and their implications for carbon cycle models. *Science* **349,** 528–532 (2015).

28. Frank, D. *et al.* Effects of climate extremes on the terrestrial carbon cycle: Concepts, processes and potential future impacts. *Glob. Chang. Biol.* **21,** 2861–2880 (2015).

29. Reyer, C. P. O. *et al.* A plant's perspective of extremes: terrestrial plant responses to changing climatic variability. *Glob. Chang. Biol.* **19,** 75–89 (2013).

30. Reichstein, M. *et al.* Climate extremes and the carbon cycle. *Nature* **500,** 287–295 (2013).

31. Luo, Y., Keenan, T. F. & Smith, M. J. Predictability of the terrestrial carbon cycle. *Glob. Chang. Biol.* **21,** 1737–1751 (2015).

32. Fisher, R. *et al.* Assessing uncertainties in a second-generation dynamic vegetation model caused by ecological scale limitations. *New Phytol.* **187,** 666–681 (2010).

33. Medvigy, D., Wofsy, S. C., Munger, J. W., Hollinger, D. Y. & Moorcroft, P. R. Mechanistic scaling of ecosystem function and dynamics in space and time: Ecosystem Demography model version 2. *J. Geophys. Res.* **114,** 1–21 (2009).

34. Scheiter, S., Langan, L. & Higgins, S. I. Next-generation dynamic global vegetation models: learning from community ecology. *New Phytol.* **198,** 957–969 (2013).

35. Fatichi, S., Leuzinger, S. & Körner, C. Moving beyond photosynthesis: from carbon source to sink-driven vegetation modeling. *New Phytol.* **201,** 1086–1095 (2014).

36. Körner, C. Paradigm shift in plant growth control. *Curr. Opin. Plant Biol.* **25,** 107–114 (2015).

37. Pappas, C., Fatichi, S., Leuzinger, S., Wolf, A. & Burlando, P. Sensitivity analysis of a process-based ecosystem model: Pinpointing parameterization and structural issues. *J. Geophys. Res. Biogeosciences* **118,** 505–528 (2013).

38. Fatichi, S., Pappas, C. & Ivanov, V. Y. Modeling plant-water interactions: an ecohydrological overview from the cell to the global scale. *Wiley Interdiscip. Rev. Water* **3,** 327–368 (2015).

39. Pugh, T. A. M., Müller, C., Arneth, A., Haverd, V. & Smith, B. Key knowledge and data gaps in modelling the influence of $CO_2$ concentration on the terrestrial carbon sink. *J. Plant Physiol.* **203,** 3–15 (2016).

40. Fernández-Martínez, M. *et al.* Nutrient availability as the key regulator of global forest carbon balance. *Nat. Clim. Chang.* **4,** 471–476 (2014).

41. Aubin, I. *et al.* Traits to stay, traits to move: a review of functional traits to assess sensitivity and adaptive capacity of temperate and boreal trees to climate change. *Environ. Rev.* **23,** 1–23 (2016).

42. Lombardozzi, D. L., Bonan, G. B., Smith, N. G., Dukes, J. S. & Fisher, R. A. Temperature acclimation of photosynthesis and respiration: A key uncertainty in the carbon cycle-climate feedback. *Geophys. Res. Lett.* **42,** 8624–8631 (2015).

43. Medlyn, B. E., Duursma, R. a. & Zeppel, M. J. B. Forest productivity under climate change: a checklist for evaluating model studies. *Wiley Interdiscip. Rev. Clim. Chang.* **2,** 332–355 (2011).

44. Potter, K. A., Arthur Woods, H. & Pincebourde, S. Microclimatic challenges in global change biology. *Glob. Chang. Biol.* **19,** 2932–9 (2013).

45. Pappas, C., Fatichi, S., Rimkus, S., Burlando, P. & Huber, M. The role of local scale heterogeneities in terrestrial ecosystem modeling. *J. Geophys. Res. Biogeosciences* **120,** 341–360 (2015).

46. Sun, Y. *et al.* Impact of mesophyll diffusion on estimated global land $CO_2$ fertilization. *Proc. Natl. Acad. Sci. U. S. A.* **111,** 15774–9 (2014).

47. Friend, A. D. *et al.* Carbon residence time dominates uncertainty in terrestrial vegetation responses to future climate and atmospheric $CO_2$. *Proc. Natl. Acad. Sci. U. S. A.* **111,** 3280–5 (2014).

48. Sulman, B. N., Phillips, R. P., Oishi,  a. C., Shevliakova, E. & Pacala, S. W. Microbe-driven turnover offsets mineral-mediated storage of soil carbon under elevated $CO_2$. *Nat. Clim. Chang.* **4,** 1099–1102 (2014).

49. Friedlingstein, P. & Prentice, I. Carbon-climate feedbacks: a review of model and observation based estimates. *Curr. Opin. Environ. Sustain.* **2,** 251–257 (2010).

50. Ault, T. R., Cole, J. E. & St. George, S. The amplitude of decadal to multidecadal variability in precipitation simulated by state-of-the-art climate models. *Geophys. Res. Lett.* **39,** 3–6 (2012).

51. Dee, D. P. *et al.* The ERA-Interim reanalysis: Configuration and performance of the data assimilation system. *Q. J. R. Meteorol. Soc.* **137,** 553–597 (2011).

52. Kalnay, E. *et al.* The NCEP/NCAR 40-year reanalysis project. *Bulletin of the American Meteorological Society* **77,** 437–471 (1996).

53. Kanamitsu, M. *et al.* NCEP-DOE AMIP-II reanalysis (R-2). *Bull. Am. Meteorol. Soc.* **83,** 1631–1643+1559 (2002).

54. Whitaker, J. S., Compo, G. P., Wei, X. & Hamill, T. M. Reanalysis before radiosondes using ensemble data assimilation. *Mon. Weather Rev.* **132,** 1190–1200 (2004).

55. Compo, G. P., Whitaker, J. S. & Sardeshmukh, P. D. Feasibility of a 100-year reanalysis using only surface pressure data. *Bull. Am. Meteorol. Soc.* **87,** 175–190 (2006).

56. Compo, G. P. *et al.* The Twentieth Century Reanalysis Project. *Q. J. R. Meteorol. Soc.* **137,** 1–28 (2011).

57. Mitchell, T. D., Carter, T. R., Jones, P. D. & Hulme, M. *A comprehensive set of high-resolution grids of monthly climate for Europe and the globe: the observed record (1901-2000) and 16 scenarios (2001-2100)*. (2004).

58. Harris, I., Jones, P. D., Osborn, T. J. & Lister, D. H. Updated high-resolution grids of monthly climatic observations - the CRU TS3.10 Dataset. *Int. J. Climatol.* **34,** 623–642 (2014).

59. Pinty, B. *et al.* Exploiting the MODIS albedos with the Two-Stream Inversion Package (JRC-TIP): 1. Effective leaf area index, vegetation, and soil properties. *J. Geophys. Res. Atmos.* **116,** 1–20 (2011).

**Figure 1.** Spatial distribution of the analysed forest sites. (a) The 23 sites with long-term (≥10 yr) micrometeorological and NEE measurements. (b) European sites where, additionally, TRW and AGB data are available (white circles). (c) Length of the analysed time series of micrometeorological and eddy covariance measurements (the five European sites with additional measurements are highlighted in black). Different colours correspond to different forest types.

**Figure 2.** Ecosystem and hydrometeorological variability based on eddy covariance and micrometeorological data, respectively. Standard deviation (y-axes) as a function of the averaging time scale (x-axes) for NEE (subplot a) as well as for the hydrometeorological drivers, namely $R$, $T$, $P$, and $D$ (subplots b, c, d, and e, respectively), from hourly to inter-annual time scales for the 23 sites (Figure 1). Data are standardized, i.e., zero mean and unit variance, at the hourly time scale, so that patterns of variability can be compared across sites. Different colours correspond to different forest types.

**Figure 3.** Composite ecosystem and hydrometeorological variability continua. (a) Ecosystem variability (y-axis) from hourly to decadal time scales of an exemplary site (DE-Tha; Figure 1b) as revealed by the superposition of several ecosystem variables (i.e., NEE, LAI and FPAR from MODIS TIP and GIMMS 3g, TRW, and AGB), and (b) its hydrometeorological envelope, based on the variability continua of individual hydrometeorological variables (i.e., $P$, $D$, $R$, $T$). Different colours correspond to different ecosystem and hydrometeorological variables. Horizontal bars highlight the time scales covered by each dataset.

**Figure 4.** The hydrometeorological envelope of ecosystem variability continuum. Single coloured solid lines merge information at multiple time scales: eddy covariance flux measurements (NEE; 1 h – 1 mon), remote sensing data (LAI 3g; 1 mon – 1 yr), and tree ring

widths (TRW; 1 yr – 10 yr) and represent the continuum of ecosystem variability at five forest ecosystems in Europe (coloured lines; Figure 1b). The shaded blue area represents the hydrometeorological envelope of variability at these five sites and it is quantified by several state-of-the-art hydrometeorological datasets (Methods; coarser increments in x-axis are used for enhancing figure's clarity).

**Figure 5.** Empirical vs. simulated continua of ecosystem variability. A comparison of observation-based (i.e., composite of NEE, LAI 3g, and TRW data; subplot a) and simulated (TRENDY multi-model mean simulated NEE; subplot b) cross-scale ecosystem variability (y-axes) across sites (coloured lines). The shaded area denotes the hydrometeorological envelope of the TRENDY climate forcing (CRU-NCEPv4). For figures' clarity, data are standardised so that they have zero mean and unit variance at the monthly time scale.

**Figure 6.** A parsimonious stochastic framework for modelling ecosystem and hydrometeorological variability across time scales. Theoretical values of standard deviation (y-axes) vs. averaging time scale (x-axes) for (a) single (deterministic) harmonics with periods T1=24 h, T2=1 yr and a process with two harmonic cycles T1 and T2; and for (b) white noise (WN) and stochastic processes with short- (AR(1)), or long-term (HK) persistence for various values of Hurst coefficient ($H$) and lag-1 autocorrelation ($\rho$). (c) Empirical ecosystem variability across time scales of an exemplary site (DE-Tha, coloured points; Figure 1b) based on eddy covariance flux measurements (NEE; 1 h – 1 mon), remote sensing data (LAI 3g; 1 mon – 1 yr), and tree ring widths (TRW, 1 yr – 10 yr; Figure 3a), together with the fitted theoretical models (dashed and solid lines; T1+T2+WN, T1+T2+AR(1), and T1+T2+HK). (d) Empirical (coloured points) and fitted theoretical (solid lines) variability across time scales for each hydrometeorological variable at DE-Tha site.

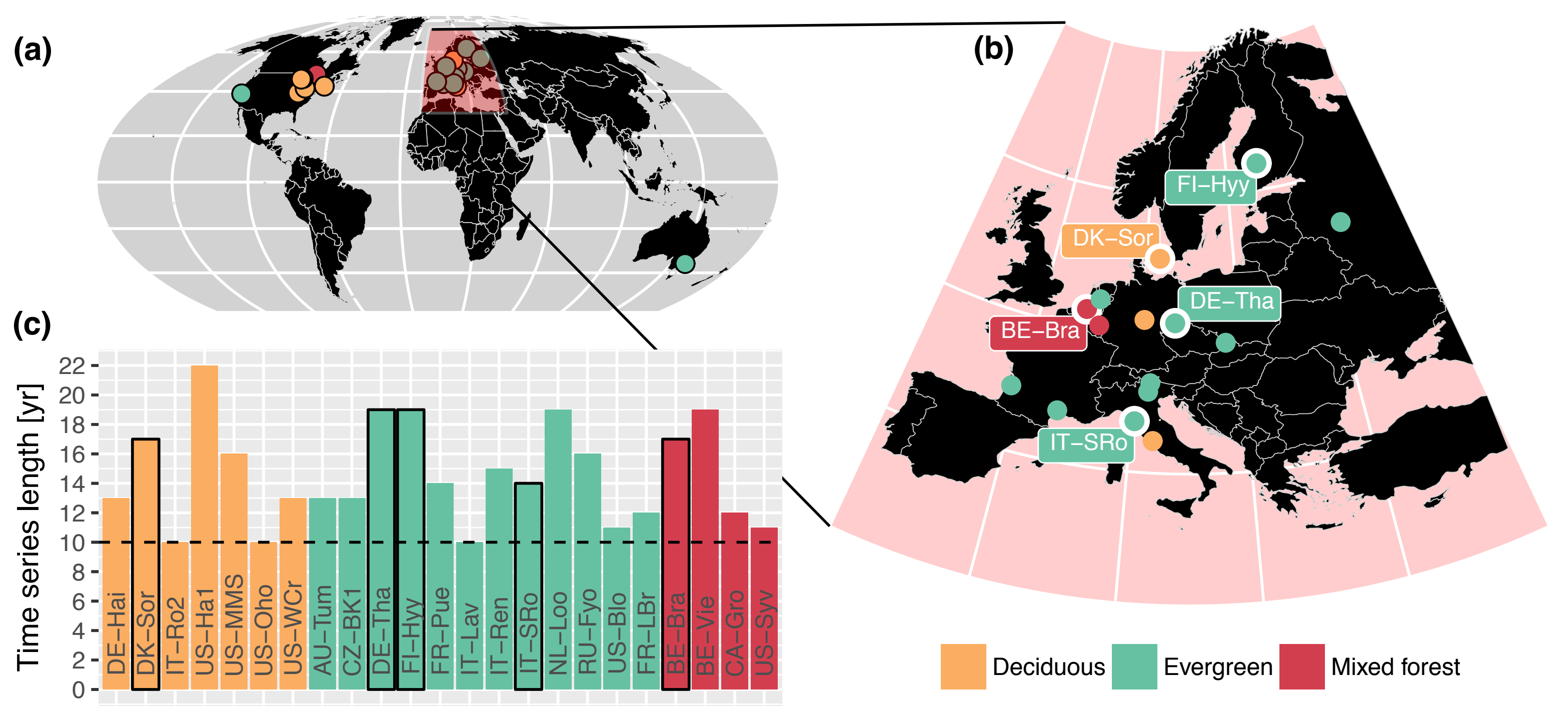

(a)
(b)
(c)
FI–Hyy
DK–Sor
DE–Tha
BE–Bra
IT–SRo
Time series length [yr]
0
2
4
6
8
10
12
14
16
18
20
22
DE–Hai
DK–Sor
IT–Ro2
US–Ha1
US–MMS
US–Oho
US–WCr
AU–Tum
CZ–BK1
DE–Tha
FI–Hyy
FR–Pue
IT–Lav
IT–Ren
IT–SRo
NL–Loo
RU–Fyo
US–Blo
FR–LBr
BE–Bra
BE–Vie
CA–Gro
US–Syv
Deciduous
Evergreen
Mixed forest

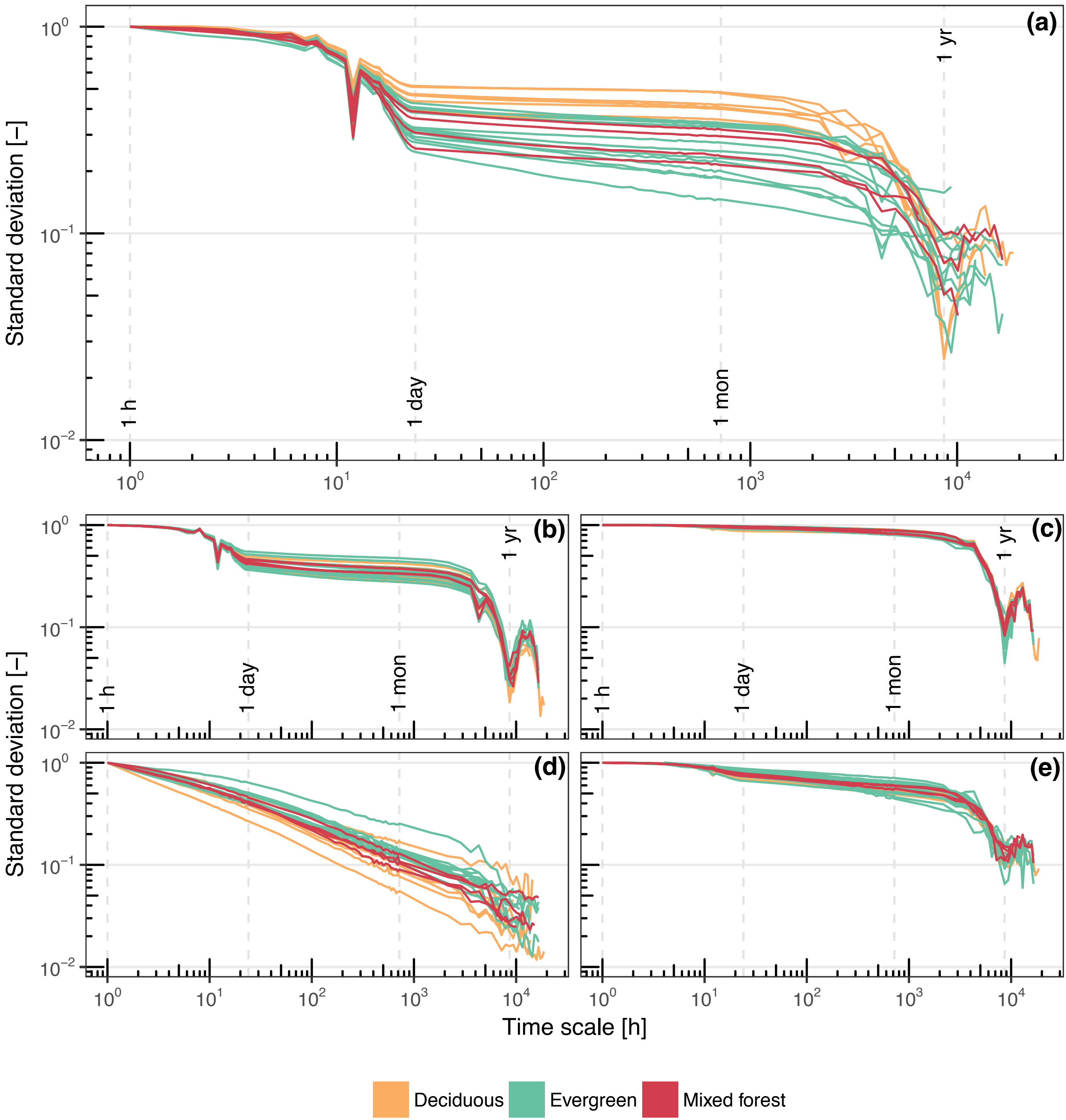

(a)
(b)
(c)
(d)
(e)
Standard deviation [–]
Time scale [h]
1 h
1 day
1 mon
1 yr
$10^{0}$
$10^{-1}$
$10^{-2}$
$10^{0}$
$10^{1}$
$10^{2}$
$10^{3}$
$10^{4}$
Deciduous
Evergreen
Mixed forest

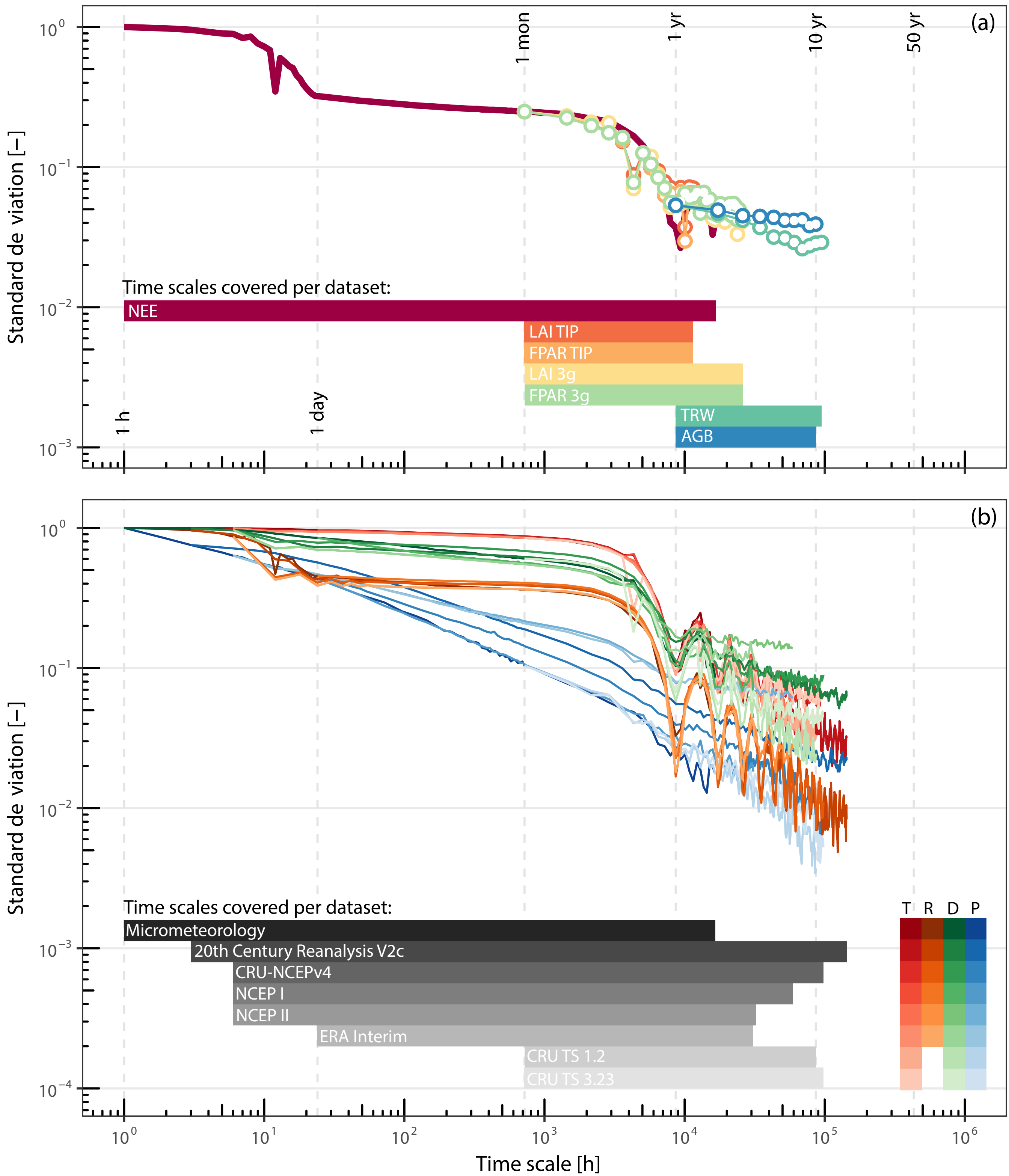
(a)
Standard de viation [–]
1 h
1 day
1 mon
1 yr
10 yr
50 yr
Time scales covered per dataset:
NEE
LAI TIP
FPAR TIP
LAI 3g
FPAR 3g
TRW
AGB
(b)
Standard de viation [–]
Time scales covered per dataset:
Micrometeorology
20th Century Reanalysis V2c
CRU-NCEPv4
NCEP I
NCEP II
ERA Interim
CRU TS 1.2
CRU TS 3.23
T R D P
Time scale [h]

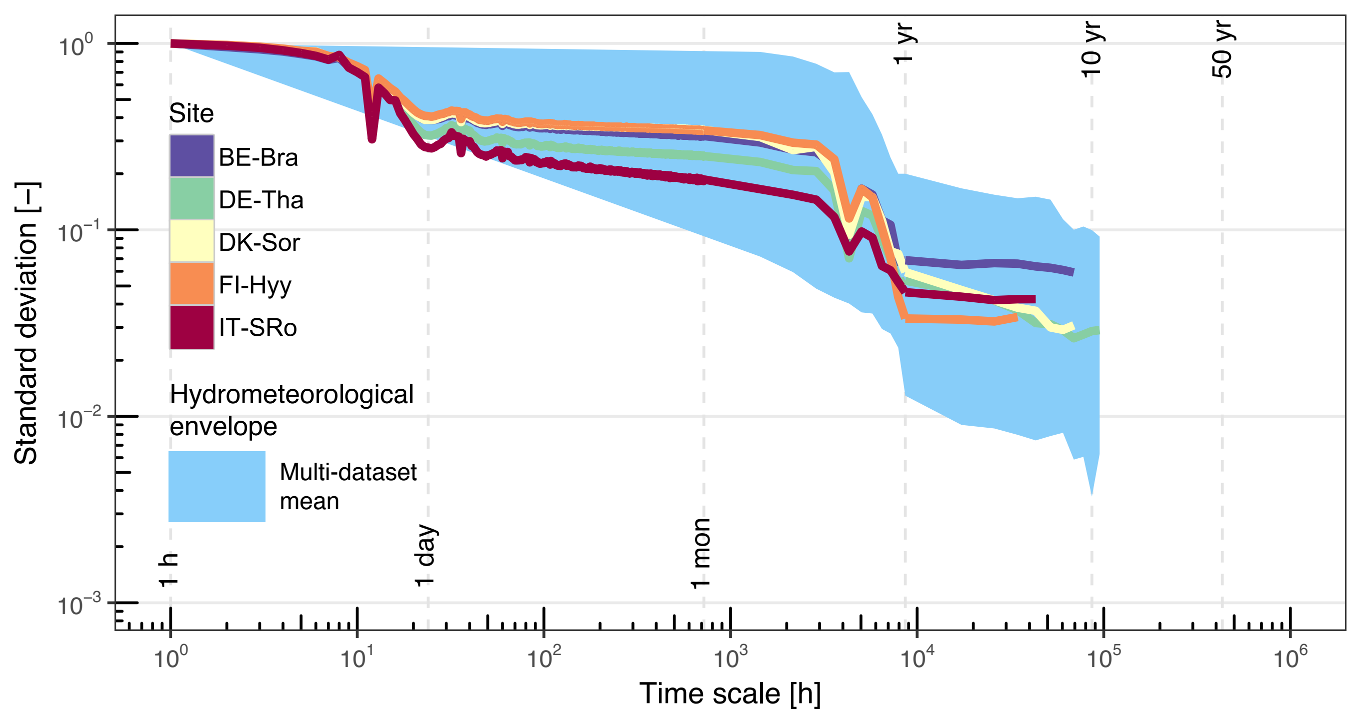

Site
BE-Bra
DE-Tha
DK-Sor
FI-Hyy
IT-SRo
Hydrometeorological envelope
Multi-dataset mean
Standard deviation [–]
Time scale [h]
1 h
1 day
1 mon
1 yr
10 yr
50 yr
$10^0$
$10^{-1}$
$10^{-2}$
$10^{-3}$
$10^0$
$10^1$
$10^2$
$10^3$
$10^4$
$10^5$
$10^6$

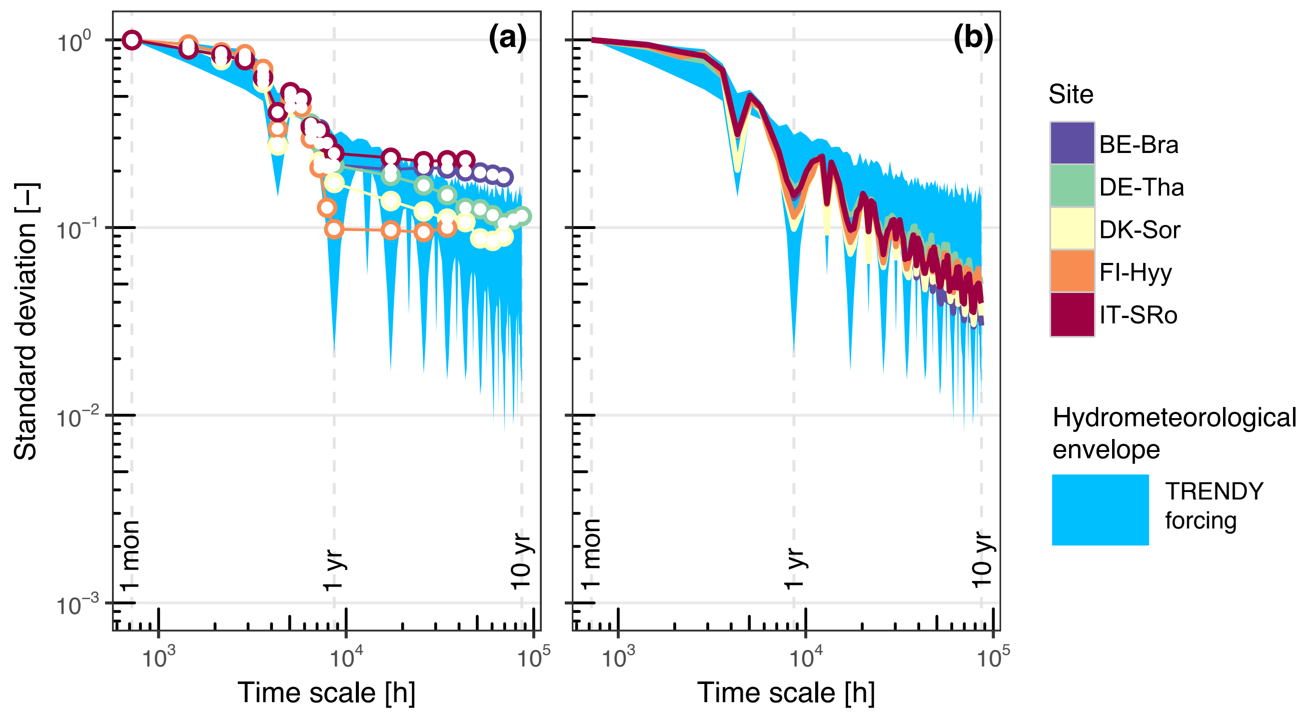

(a)
(b)
Standard deviation [–]
$10^0$
$10^{-1}$
$10^{-2}$
$10^{-3}$
$10^3$
$10^4$
$10^5$
Time scale [h]
1 mon
1 yr
10 yr
Site
BE-Bra
DE-Tha
DK-Sor
FI-Hyy
IT-SRo
Hydrometeorological envelope
TRENDY forcing

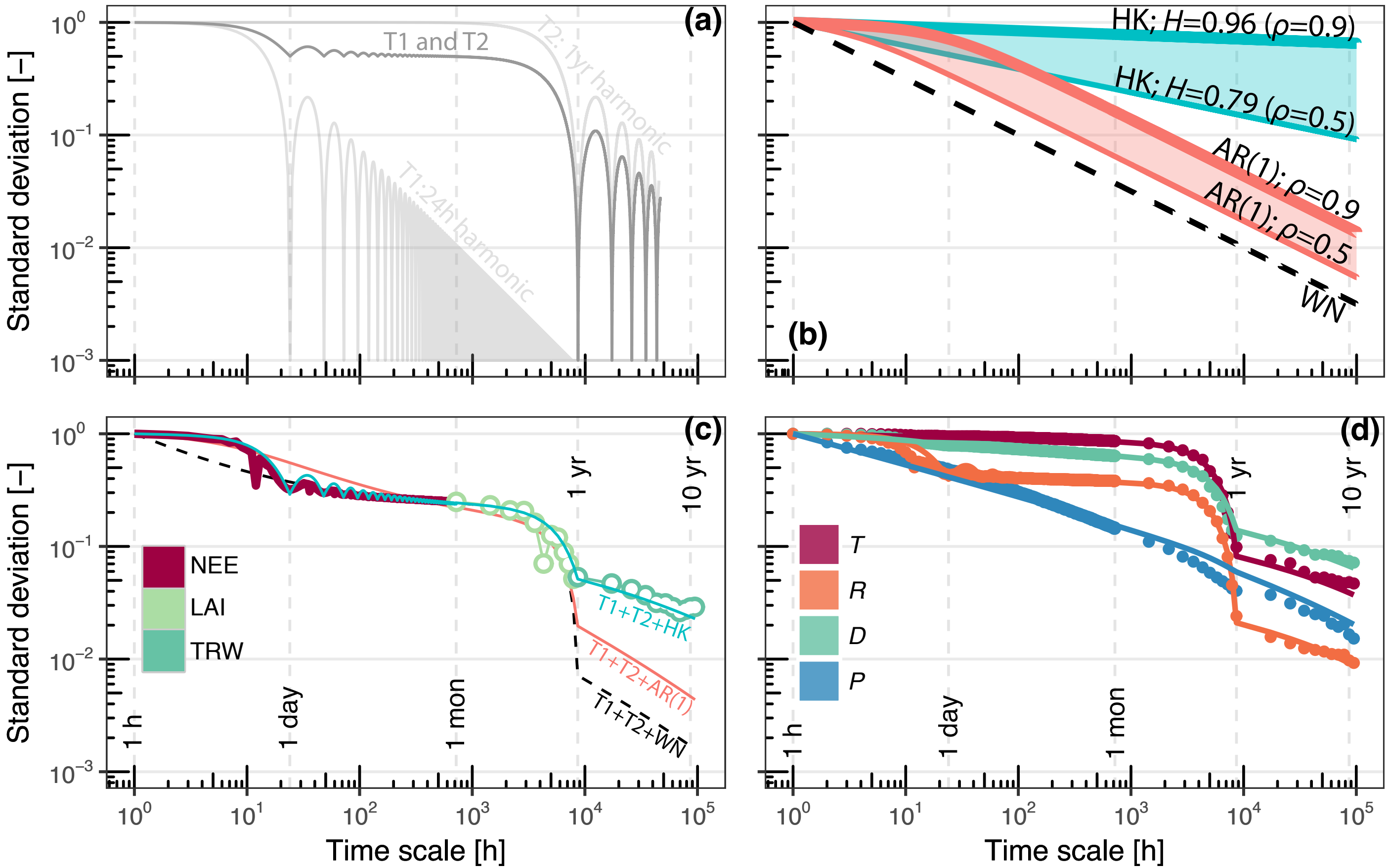

(a)
T1 and T2
T2: 1yr harmonic
T1:24h harmonic
(b)
HK; H=0.96 (ρ=0.9)
HK; H=0.79 (ρ=0.5)
AR(1); ρ=0.9
AR(1); ρ=0.5
WN
(c)
NEE
LAI
TRW
T1+T2+HK
T1+T2+AR(1)
T1+T2+WN
1 h
1 day
1 mon
1 yr
10 yr
(d)
T
R
D
P
Standard deviation [–]
Time scale [h]